SciEn

Proceedings of 8th International Conference on Mechanical, Industrial and Energy Engineering 2024
02-04 January, 2025, Khulna, BANGLADESH

SciEn Conference Series: Engineering Vol. 3, 2025, pp 31-36 https://doi.org/10.38032/scse.2025.3.9

Numerical Analysis of Bubble Dynamics in Bifurcation Vessels with Stenosis and Varying Bifurcation Angle

Ratul Das and Md. Mamunur Roshid*

Department of Mechanical Engineering, Chittagong University of Engineering & Technology, Chattogram-4349, Bangladesh

ABSTRACT

In this study, a numerical investigation was conducted into the transport and splitting behavior of perfluorocarbon (PFC) bubbles within bifurcating arterial networks, with a focus on gas embolotherapy, a potential cancer treatment. A two-dimensional arterial model was used to examine how blood flow affects bubble dynamics. The volume of fluid (VOF) method in computational fluid dynamics (CFD) simulations was employed to model the interaction between capsular-shaped bubbles and blood flow. Multiple bifurcation angles, 60° and 90°, were analyzed, both with and without stenosis, to assess their impact on bubble movement and splitting phenomena. The results demonstrated that both bifurcation angle and stenosis significantly affected bubble behavior. In the 60° and 90° bifurcation vessels without stenosis, the bubble split homogeneously and traveled through the entire vessel path. However, in the 60° bifurcation vessel with stenosis, the bubble did not split homogeneously and passed through only one daughter artery. In contrast, the bubble split homogeneously in the 90° bifurcation vessel with stenosis. These findings provide valuable insights into how vessel geometry impacts bubble movement and splitting in blood and contribute to optimizing gas embolotherapy treatments.

Keywords: Bubble Dynamics; Non-Newtonian blood flow; Numerical solution; Bifurcation and stenosis.

1 Introduction

Gas embolotherapy has emerged as an effective treatment strategy for cancer, specifically targeting the disruption of blood flow to tumors through the precise injection of gas bubbles. This approach, which builds on the foundational research of Bull and Wong [1], [2], [3] involves the use of micron-sized fluoropentane (C_5F_{12}) droplets that are encapsulated in albumin or lipid shells to delay bubble formation. These droplets, which have a low boiling point, traverse the bloodstream until externally activated. Under the influence of high-intensity ultrasound, the droplets undergo Acoustic Droplet Vaporization (ADV), causing them to rapidly expand into gas bubbles. This process occurs at the tumor site, leading to occlusion of the blood vessels and subsequent ischemia, particularly in the microcirculatory system, which ultimately results in tissue infarction. However, for gas embolotherapy to be successful, effective management of bubble dynamics and distribution within the vascular system is crucial. Previous studies [4], [5] have improved our understanding of bubble transport within bifurcation models, identifying critical factors that affect bubble lodging and occlusion of blood vessels. This paper seeks to build on that knowledge by exploring new methods to optimize gas embolotherapy for more effective tumor targeting and enhanced therapeutic outcomes.

While many studies have focused on bifurcation models, real-world arterial conditions often include stenosis, or narrowing of the blood vessels, which can further influence blood flow and bubble dynamics. To achieve a more accurate representation of arterial conditions, this study includes stenosis in combination with bifurcation angles to investigate their collective impact on bubble behavior. Poornima and Vengadesan (2012) investigated bubble dynamics in microchannels designed to replicate human arterioles, highlighting variations in splitting ratios between symmetrical and asymmetrical channels [6]. Qamar et al. (2017) expanded on this work by pinpointing critical factors, such as gravitational imbalances and bifurcation vortices, that influence bubble splitting and exert shear stress on vessel walls, which could impact the health of endothelial cells [7]. Similarly, Nagargoje and Gupta (2020, 2023) analyzed the role of fluid properties, flow rates, and bifurcation geometry in bubble behavior within Y-shaped channels, observing that splitting behavior changes significantly with different Reynolds numbers[8], [9].

Research on bubble dynamics in blood flow has predominantly focused on Newtonian fluids, with limited exploration of how non-Newtonian properties of blood influence bubble behavior. Examining the impact of blood's non-Newtonian nature could offer important insights into bubble behavior under more realistic physiological conditions. Unlike in Newtonian fluids, bubbles in non-Newtonian blood flow interact with red blood cells and other cellular components, leading to distinct behavioral patterns. Although some aspects of this interaction have been investigated, further research is needed to better understand the effects of non-Newtonian blood flow on bubble dynamics. This study aims to fill this gap by examining the behavior of PFC bubbles in stable non-Newtonian blood flow within two-dimensional, symmetric bifurcating networks, using bifurcation angles of 60° and 90° to analyze various bubble arrangements.

*Corresponding Author Email Address: ratuldasctg03@gmail.com

2 Research Methodology

A two-dimensional model of the arterial network (Fig. *1*) was created using computer-aided design (CAD) tools. To simulate blood as a non-Newtonian fluid, the power-law rheological model was applied, which describes the correlation between shear stress and shear rate. The parameters for the model—specifically the consistency index (K) and the flow behavior index (n)-were determined experimentally using blood samples, as reported by Kopernik and Tokarczyk [10]. For the purposes of this study, the consistency index (K) was set to 0.13, while the flow behavior index (n) was assigned a value of 0.7. The secondary phase in the model consists of perfluorocarbon (PFC) gas, with a density of 12 kg/m^3 and viscosity of 2×10^{-5} Pa·s [6]. These values were incorporated into the computational fluid dynamics (CFD) simulations using the power-law model.

The geometry of the arterial network in the CFD simulations is based on defined vessel diameters. The mother artery diameter is 1 mm, and the daughter arteries diameters are 0.78 mm respectively [8]. To explore various bifurcation configurations, the bifurcation angles, α and β, were symmetrically adjusted between 60° and 90° (Fig. *1*). In addition, a 60% stenosis was introduced in the mother vessel in some simulations to evaluate its influence on bubble dynamics (Fig. *2*). In all simulations, a capsular bubble with a diameter of 0.79 mm and a height of 0.5 mm was used to examine its shape and behavior during the simulations.

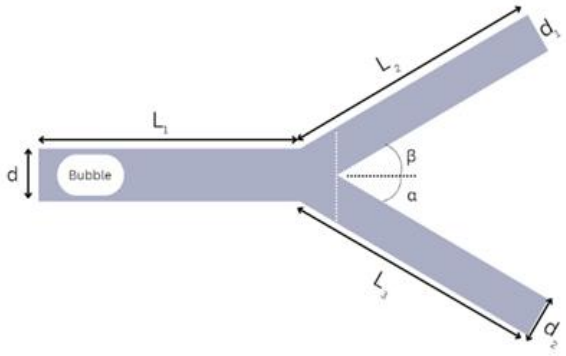

Fig. 1 Diagram showing the geometry of bifurcation, where mother artery d = 1 mm, daughter arteries are d_1, d_2 = 0.78 mm, length L_1, L_2, L_3 = 5d, and α, β are the angles between the daughter and mother arteries.

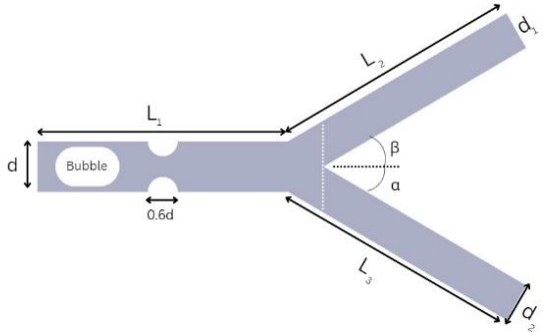

Fig. 2 Diagram showing the bifurcation geometry with 60% stenosis at the center of the mother artery.

2.1 Numerical Modeling

The movement of perfluorocarbon (PFC) bubbles through bifurcated and stenosed artery models presents a complex challenge involving gas-liquid multiphase flow, where blood is treated as a non-Newtonian fluid. This study uses the Volume of Fluid (VOF) method, based on the continuum surface force (CSF) model, within the finite-volume-based commercial computational fluid dynamics (CFD) software ANSYS Fluent 2023R2(Student edition). The VOF method is favored for its precision, adaptability, and stability in simulating multiphase flows, as it solves a single set of momentum equations for all phases involved.

The geometric configuration was implemented in the CFD simulations, with the angles systematically varied between 30° and 45° (Fig. *1*).

The governing equations for the VOF model are as follows:

1. Equation of Continuity:

$$\boldsymbol{\nabla}\cdot\boldsymbol{u}=0 \tag{1}$$

2. Equation of Momentum Conservation:

$$\rho\left(\frac{\partial \boldsymbol{u}}{\partial t}+(\boldsymbol{u}\cdot\nabla)\boldsymbol{u}\right)=-\boldsymbol{\nabla}P+\boldsymbol{\nabla}\cdot\tau+\boldsymbol{F} \tag{2}$$

3. Shear Stress Tensor:

$$\tau=\mu(\nabla\boldsymbol{u}+(\nabla\boldsymbol{u})^T) \tag{3}$$

4. Volume Fraction Equation:

$$\frac{\partial a_G}{\partial t}+u\cdot\nabla a_G=0 \tag{4}$$

The mixture density ρ, and viscosity μ are determined using the volume fractions of the two phases:

$$\rho=\alpha_L\rho_L+\alpha_G\rho_G \tag{5}$$

$$\mu=\alpha_L\mu_L+\alpha_G\mu_G \tag{6}$$

The body force Term F in equation (2) includes the surface tension force σ, which is expressed using the CSF model as proposed by Brickbill et al. [11]:

$$\boldsymbol{F}=\sigma\kappa\boldsymbol{n} \tag{7}$$

where κ is the curvature and can be calculated as:

$$\kappa=\nabla\cdot\hat{n} \tag{8}$$

where n is the normal vector, defined as:

$$\boldsymbol{n}=\boldsymbol{\nabla\alpha} \tag{9}$$

And the unit normal vector is given:

$$\hat{\boldsymbol{n}}=\frac{\boldsymbol{n}}{|n|} \tag{10}$$

The artery model is meshed using ANSYS Meshing, and a mesh independence study is performed to ensure the accuracy of the results. In the bifurcating artery model, blood is modeled as the primary liquid phase, while the PFC bubble serves as the secondary gas phase. The bubble is placed 1 mm from the inlet, with a surface tension of 0.05 N/m between the blood and the PFC bubble. The Reynolds number, based on the diameter of the mother vessel, is set to 100.

For unsteady-state simulations, a parabolic inlet velocity profile is used, with a constant Reynolds number of 100, and a zero-gauge pressure boundary condition is applied at the outlet. The pressure-velocity coupling is solved using the

Pressure Implicit with Splitting of Operator (PISO) method, with pressure interpolation incorporating the body-force-weighted scheme. The momentum equations are discretized using the quadratic upwind interpolation for convection kinetics (QUICK) method, and a sharp interface between phases is maintained using the High-Resolution Interface Capturing (HRIC) scheme. The unsteady term is discretized using a first-order implicit time-marching scheme, and the simulations advance with a time step of 1×10^{-6} s to accurately capture the system's dynamic behavior.

3 Results and Discussion

When the bifurcation angle is 60°, the mother vessel initially experiences a pressure surge along its interior, which gradually subsides as the bubble moves forward. As the bubble advances, it undergoes shape changes, with the front part becoming convex and the rear part concave (at t = 6.9 ms), as shown in Fig. 3. This shape change continues until the bubble reaches the bifurcation junction, where it deforms further (at t = 10.475 ms), resulting in a flattened front and convex rear. The bubble starts to divide around t = 13.425 milliseconds (Fig. 3) when it interacts with the bifurcation points, causing the daughter vessels to become blocked by the newly formed bubbles.

Interestingly, the pressure inside the mother artery is initially high but gradually decreases and stabilizes as the bubble reaches the bifurcation region. At the intersection, an increase in pressure behind the bubble facilitates its forward motion. After the bubble passes through the bifurcation, the pressure stabilizes.

The velocity distribution behind the bubble exhibits distinct patterns as well. At t = 6.9 ms (refer to Fig. 3), the velocity behind the bubble reaches its maximum, aiding its propulsion. When the bubble approaches the junction (t = 10.475 ms, as shown in Fig. 3, its interaction with the upper and lower artery walls results in a velocity reduction both in front of and behind the bubble. At the bifurcation (illustrated in
Fig. 3), the velocity is notably low, with blood flowing around the bubble. As the bubble begins to split, the velocity gradually increases (t = 15.743 ms).

For the 90° bifurcation, the bubble exhibits behavior similar to that seen in the 60° configuration. (Fig. 4). The pressure dynamics in the 90° bifurcation are comparable to those in the 60° configuration, with pressure levels remaining steady or showing slight increases relative to the earlier case. The bubble demonstrates consistent deformation and splitting behavior, indicating uniform patterns across the bifurcation angles.

Similarly, the velocity profile of the bubble in the 90° bifurcation mirrors that observed in the 60° bifurcation. This consistency in velocity distribution across bifurcation configurations underscores the robustness of the phenomena, suggesting that the bubble's behavior remains unaffected by changes in bifurcation angle.

When stenosis is introduced within the 60° bifurcation artery, the bubble initially retains a capsular shape but begins to deform as it approaches the stenosis. By the time the bubble is situated midway through the stenosis (t = 2.55 ms) as depicted in Fig. 5, its shape transforms into a dumbbell-like form.

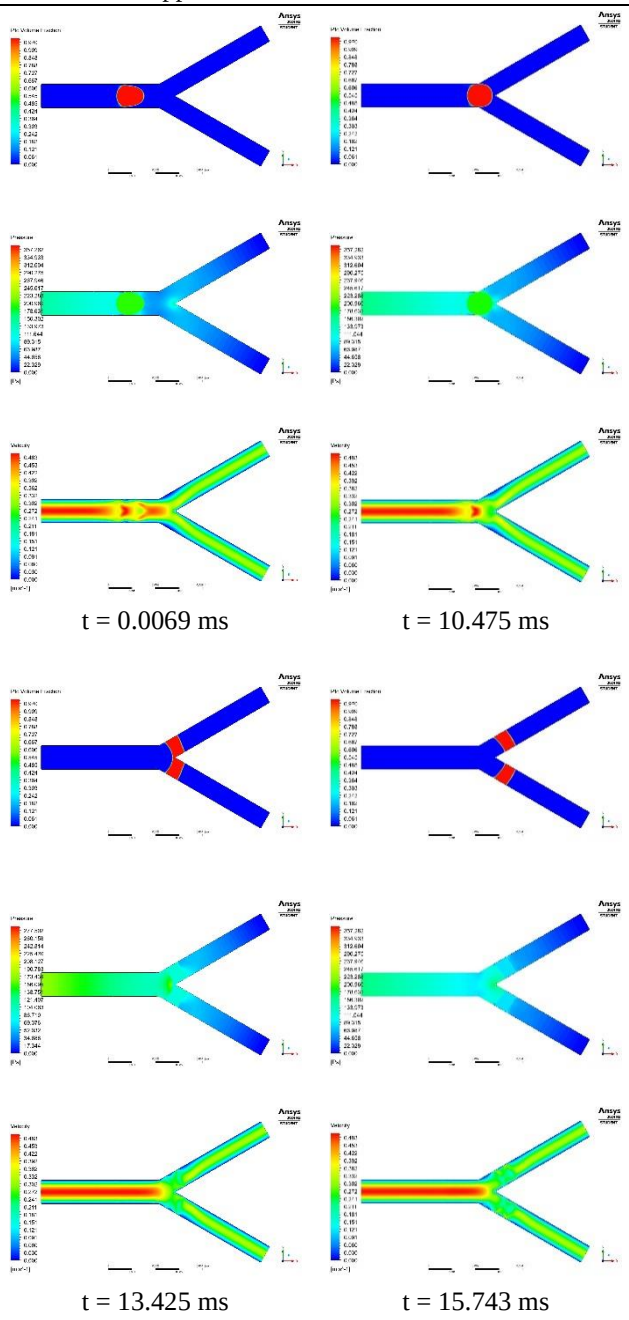

Fig. 3 Bubble (top), pressure (center), and velocity (bottom) contours at different time intervals for a bubble advancing towards the bifurcation angle of $\alpha = \beta = 30°$

The rear section of the bubble adheres to the stenosis wall, and as it advances, small segments of the bubble, termed satellites, also cling to the walls. Upon reaching the bifurcation junction, the bubble becomes increasingly unstable, tilting toward the upper arterial wall. At t = 10.44 ms (Fig. 5), as the bubble makes contact with the bifurcation point, it adheres to the upper wall and progresses forward. By t = 12.25 ms, the majority of the bubble remains attached to the upper wall, while a smaller portion clings to the lower wall.

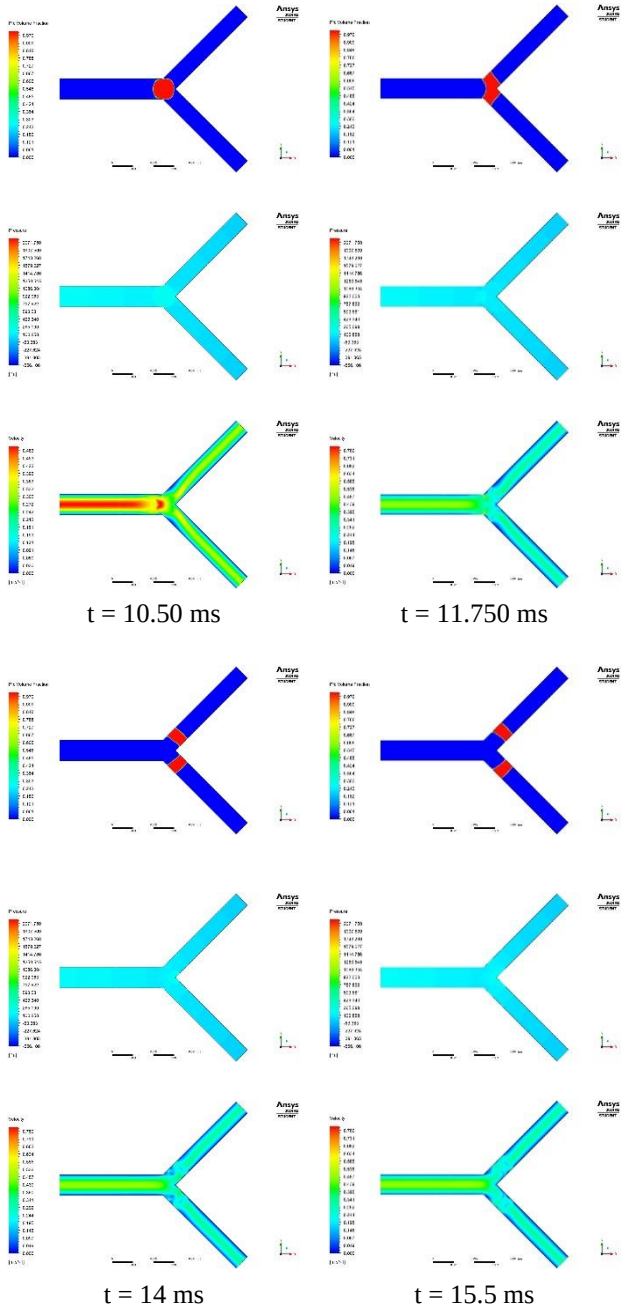

Fig. 4 Bubble (top), pressure (center), and velocity (bottom) contours at different time intervals for a bubble advancing towards the bifurcation angle of $\alpha = \beta = 45$

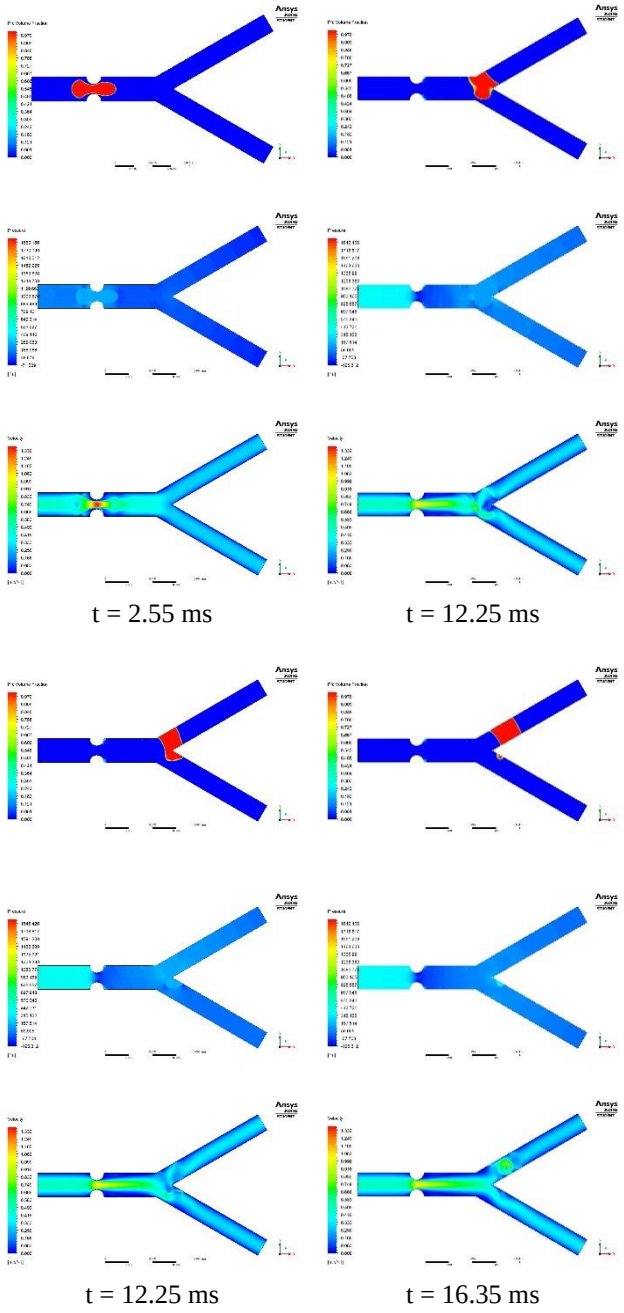

Fig. 5 Bubble (top), pressure (center), and velocity (bottom) contours at different time intervals for a bubble advancing towards the bifurcation angle with stenosis of $\alpha = \beta = 45°$

This results in an asymmetric division of the bubble at the bifurcation point, and by t = 16.35 ms, the bubble has fully entered the daughter artery.

In terms of velocity, the magnitude is highest just before the bubble encounters the stenosis, peaking in the center of the narrowed section (Fig. 5). However, as the bubble traverses the stenosis, the velocity decreases. Prior to crossing the stenosis, the velocity is high throughout the bifurcation artery but gradually diminishes as the bubble reaches the junction and begins to split into the daughter arteries. Once the bubble has positioned itself within the upper daughter artery, a medium velocity magnitude can be observed in that region.

Regarding pressure, the levels are notably high before the bubble enters the stenosis. As the bubble passes through, there is a slight reduction in pressure, though it remains relatively elevated across the bifurcation artery, maintaining the necessary force to propel the bubble forward. Once the bubbles have split and reside within the daughter arteries, the surrounding pressure stabilizes at a moderate level.

In the scenario involving a 90° bifurcation angle and stenosis, the initial bubble behavior mirrors that observed in the 60° bifurcation, up until the bubble reaches the bifurcation intersection. At this point, a noticeable difference occurs. Unlike the 60° case, where the bubble only makes contact with the upper wall, in the 90° bifurcation, the bubble touches both lower walls simultaneously at t = 10.35 ms (as illustrated in Fig. 6) before advancing.

As the bubble reaches the bifurcation point, it begins to split, and by t = 12 ms, the bubble has evenly divided between the daughter arteries. The symmetrical movement of the bubble continues, and by t = 14.045 ms, it has fully entered the daughter arteries.

Regarding velocity, similar patterns to the 60° bifurcation are observed throughout most of the process. However, when the bubbles settle into the two daughter arteries, there is no noticeable variation in velocity.

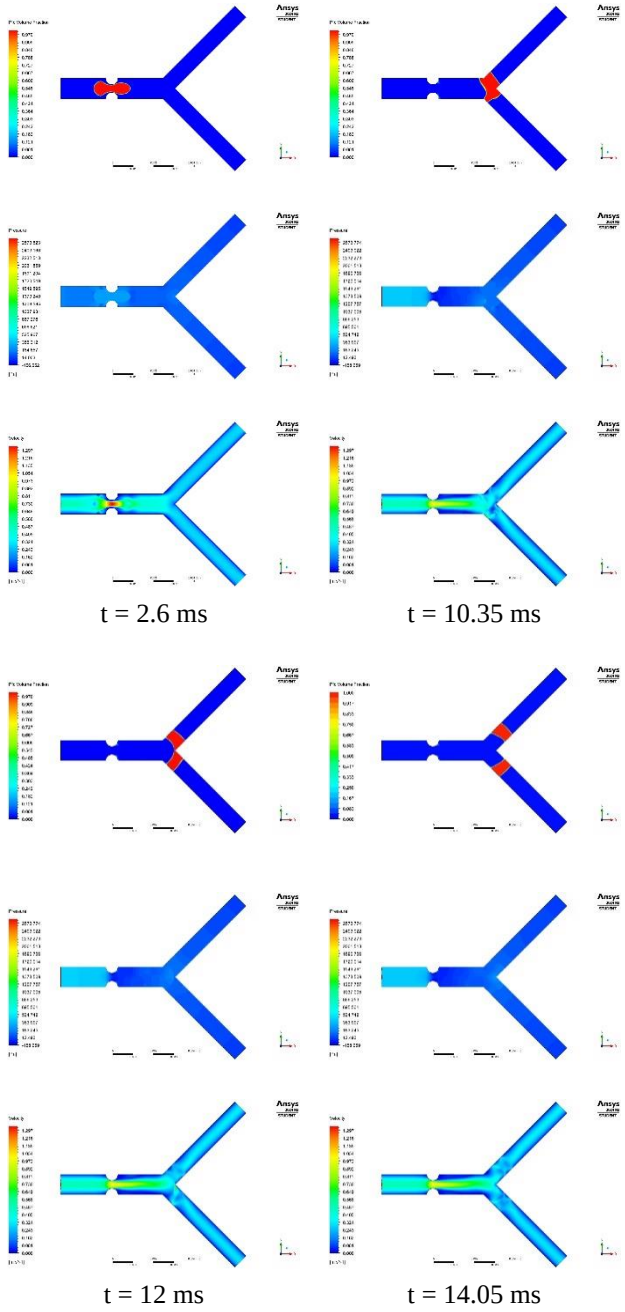

Fig. 6 Bubble (top), pressure (center), and velocity (bottom) contours at different time intervals for a bubble advancing towards the bifurcation angle with stenosis of $\alpha = \beta = 45°$

The pressure dynamics also show no substantial deviation from the 60° bifurcation case. While there are minor fluctuations in pressure magnitude, the overall pressure remains higher before the stenosis. Once the bubbles have split and reside within the daughter arteries, the pressure between the bubbles and the stenosis remains slightly elevated.

4 Scope and Limitation

This study aims to explore bubble splitting behavior and assess the influence of non-Newtonian blood properties on perfluorocarbon (PFC) bubble dynamics using a two-dimensional arterial model and computational fluid dynamics (CFD).

However, certain limitations exist. The two-dimensional model restricts the analysis depth, suggesting future studies should adopt three-dimensional geometries to better capture real vascular conditions. Additionally, arterial walls were considered rigid, overlooking the effects of wall compliance—an important aspect of actual arteries. The fixed bifurcation angles and specific stenosis configurations limit variability, and future work should explore more anatomically accurate and diverse geometries.

The study uses the non-Newtonian power-law model for blood viscosity, which may not fully capture the complexity of blood behavior. Incorporating other rheological models, such as Bingham, Hershel-Bulkley or Carreau-Yasuda, could enhance understanding. Furthermore, pulsatile flow was not modeled, omitting the natural oscillations of arterial blood flow that significantly impact bubble behavior.

5 Conclusion

The simulation results provide valuable insights into the behavior of capsular bubbles as they approach bifurcation angles of 60° and 90°, both with and without the presence of stenosis. The findings reveal consistent deformation patterns and pressure dynamics across different bifurcation configurations, demonstrating that bubble morphology changes, such as convex leading and concave trailing edges, are stable regardless of the bifurcation angle. However, notable differences emerge in bubble behavior at bifurcation junctions, where the presence of stenosis induces more pronounced deformations and asymmetrical splitting.

For bifurcation vessels without stenosis, the bubbles successfully travel the entire path, consistently undergoing homogenous splitting at both 60° and 90° bifurcations. These symmetrical division behaviors highlight the robustness of bubble dynamics in unobstructed vessels, ensuring a predictable propagation into the daughter arteries.

In scenarios involving stenosis, differences become more pronounced. At both 60° and 90° bifurcation angles, the bubbles still manage to traverse the entire path, but they demonstrate asymmetrical splitting, resulting in uneven division between the daughter arteries. Importantly, in both stenosis cases, the occlusion of blood flow reaches at least 78% in one of the daughter arteries, aligning with the requirements for effective gas embolotherapy[8]. These findings indicate the potential efficacy of embolotherapy even under complex bifurcation conditions.

The pressure within the mother artery follows a predictable trend, initially high, gradually decreasing, and stabilizing once the bubble enters the bifurcation region. In cases with stenosis, pressure remains elevated before the stenosis but decreases slightly as the bubble passes through. Velocity distribution exhibits similar trends, peaking before stenosis and bifurcation points and gradually diminishing afterward, aligning with the observed deformation and division of the bubble.

These findings have important implications for gas embolotherapy, where effective occlusion of at least 78% of the blood flow is crucial for success. Understanding the

dynamics of bubble behavior in different bifurcation geometries and stenosis conditions could help optimize the conditions necessary for efficient blood flow occlusion in therapeutic applications.

References

[1] J. L. Bull, "Cardiovascular Bubble Dynamics," *Crit Rev Biomed Eng*, vol. 33, no. 4, pp. 299–346, 2005, doi: 10.1615/CritRevBiomedEng.v33.i4.10.

[2] J. L. Bull, "The application of microbubbles for targeted drug delivery," *Expert Opin Drug Deliv*, vol. 4, no. 5, pp. 475–493, Sep. 2007.

[3] Z. Z. Wong and J. L. Bull, "Vascular bubbles and droplets for drug delivery," *J Drug Deliv Sci Technol*, vol. 21, no. 5, pp. 355–367, 2011.

[4] A. J. Calderón *et al.*, "Microfluidic model of bubble lodging in microvessel bifurcations," *Appl Phys Lett*, vol. 89, no. 24, Dec. 2006.

[5] B. Eshpuniyani, J. B. Fowlkes, and J. L. Bull, "A bench top experimental model of bubble transport in multiple arteriole bifurcations," *Int J Heat Fluid Flow*, vol. 26, no. 6, pp. 865–872, Dec. 2005.

[6] J. Poornima and S. Vengadesan, "Numerical Simulation of Bubble Transport in a Bifurcating Microchannel: A Preliminary Study," *J Biomech Eng*, vol. 134, no. 8, Aug. 2012

[7] A. Qamar, M. Warnez, D. T. Valassis, M. E. Guetzko, and J. L. Bull, "Small-bubble transport and splitting dynamics in a symmetric bifurcation," *Comput Methods Biomech Biomed Engin*, vol. 20, no. 11, pp. 1182–1194, Aug. 2017.

[8] M. S. Nagargoje and R. Gupta, "Numerical simulation of bubble transport and splitting dynamics for varying bifurcation angle," in *14th International Conference on CFD in 6 Oil & Gas, Metallurgical and Process Industries SINTEF, Trondheim, Norway, October 12–14, 2020*, SINTEF Academic Press, Oct. 2020.

[9] M. S. Nagargoje and R. Gupta, "Experimental investigations on the bubble dynamics in a symmetric bifurcating channel," *International Journal of Multiphase Flow*, vol. 159, p. 104318, Feb. 2023.

[10] M. Kopernik and P. Tokarczyk, "Development of multi-phase models of blood flow for medium-sized vessels with stenosis," *Acta Bioeng Biomech*, vol. 21, no. 2, pp. 63–70, 2019.

[11] J. U. Brackbill, D. B. Kothe, and C. Zemach, "A continuum method for modeling surface tension," *J Comput Phys*, vol. 100, no. 2, pp. 335–354, Jun. 1992.

NOMENCLATURE

ρ Mass density (kg/m^3)
μ Dynamic viscosity (kg/m.s)
σ Surface tension force, (N/m)
τ Shear stress tensor (N/m2)
p Pressure (Pa)
u Velocity (m/s)
κ Curvature (m-1)